Atmos. Chem. Phys. Discuss., 12, 31725–31765, 2012
www.atmos-chem-phys-discuss.net/12/31725/2012/
doi:10.5194/acpd-12-31725-2012

Atmospheric Chemistry and Physics Discussions

Secondary organic aerosol formation from gasoline passenger vehicle emissions investigated in a smog chamber

E. Z. Nordin[1], A. C. Eriksson[2], P. Roldin[2], P. T. Nilsson[1], J. E. Carlsson[1], M. K. Kajos[3], H. Hellén[4], C. Wittbom[2], J. Rissler[1], J. Löndahl[1], E. Swietlicki[2], B. Svenningsson[2], M. Bohgard[1], M. Kulmala[2,3], M. Hallquist[5], and J. Pagels[1]

[1]Ergonomics and Aerosol Technology, Lund University, P.O. Box 118, 221 00 Lund, Sweden
[2]Division of Nuclear Physics, Lund University, P.O. Box 118, 221 00 Lund, Sweden
[3]Department of Physics, University of Helsinki, P.O. Box 64, 00014 Helsinki, Finland
[4]Finnish Meteorological Institute, P.O. Box 503, 00101 Helsinki, Finland
[5]Department of Chemistry, Atmospheric Science, University of Gothenburg,
412 96 Gothenburg, Sweden

Received: 14 November 2012 – Accepted: 28 November 2012
– Published: 11 December 2012

Correspondence to: E. Z. Nordin (erik.nordin@design.lth.se)

Published by Copernicus Publications on behalf of the European Geosciences Union.

Abstract

Gasoline vehicles have elevated emissions of volatile organic compounds during cold starts and idling and have recently been pointed out as potentially the main source of anthropogenic secondary organic aerosol (SOA) in megacities. However, there is a lack of laboratory studies to systematically investigate SOA formation in real-world exhaust. In this study, SOA formation from pure aromatic precursors, idling and cold start gasoline exhaust from one Euro II, one Euro III and one Euro IV passenger vehicles were investigated using photo-oxidation experiments in a 6 m^3 smog chamber. The experiments were carried out at atmospherically relevant organic aerosol mass concentrations. The characterization methods included a high resolution aerosol mass spectrometer and a proton transfer mass spectrometer. It was found that gasoline exhaust readily forms SOA with a signature aerosol mass spectrum similar to the oxidized organic aerosol that commonly dominates the organic aerosol mass spectra downwind urban areas. After 4 h aging the formed SOA was 1–2 orders of magnitude higher than the Primary OA emissions. The SOA mass spectrum from a relevant mixture of traditional light aromatic precursors gave $f43$ (mass fraction at $m/z = 43$) approximately two times higher than to the gasoline SOA. However O : C and H : C ratios were similar for the two cases. Classical C_6–C_9 light aromatic precursors were responsible for up to 60 % of the formed SOA, which is significantly higher than for diesel exhaust. Important candidates for additional precursors are higher order aromatic compounds such as C_{10}, C_{11} light aromatics, naphthalene and methyl-naphthalenes.

1 Introduction

The formation mechanisms, magnitude and chemical composition of secondary organic aerosol (SOA) are of importance for predicting future climate scenarios (Monks et al., 2009; Hallquist et al., 2009). SOA is formed from low vapor pressure reaction products, which originate from gas phase oxidation of volatile organic compounds

(VOCs). De Gouw and Jimenez (2009) suggested that SOA from urban sources may be the dominating source of organic aerosol globally between the 30th and 50th latitude.

Traditionally the VOCs responsible for the majority of urban SOA formation have been assumed to be light aromatic hydrocarbons, which are hydrocarbons with one benzene ring, often with one or more alkyl groups (methyl, ethyl or propyl), i.e. benzene (C_6), toluene (C_7), xylenes and ethyl benzene (C_8), C_9 and C_{10} aromatics (Odum et al., 1997).

Robinson et al. (2007) recognized intermediate volatility organic compounds (IVOCs) and semi volatility organic compounds (SVOCs) as important sources for production of ambient organic aerosol. Photo-oxidation experiments of exhaust from a diesel generator indicated that only a small fraction of the SOA formed originated from light aromatic precursors (Weitkamp et al., 2007). They also suggested that IVOCs such as long chain and branched alkanes could be responsible for a large fraction of the SOA produced from diesel exhaust. However, recent smog chamber studies suggest that the SOA formation from modern diesel vehicles with functioning oxidation catalysts is very low (Chirico et al., 2010; Samy and Zielinska, 2010).

Less attention has been paid to SOA formation from gasoline exhaust, although VOC emissions can be high during cold starts, increasing with decreasing ambient temperature. At ambient temperatures below 0 °C the VOC emissions from the startup-phase can be equivalent to thousands of driven kilometers (Weilenmann et al., 2009). This is due to fuel condensing on the inner surface of the cylinder when the engine temperature is low, causing a fuel rich incomplete combustion but also because the operation temperature of the oxidation catalyst is below its optimum range (Schifter et al., 2010). The emissions from passenger gasoline vehicles may also contain ammonia which is formed as a reaction product when NO is reduced on catalytic surfaces in catalytic converters (Heeb et al., 2006; Kean et al., 2009). Gasoline exhaust contains a complex mixture of VOCs, nitrogen oxides (NO_x), ammonia and particulate matter (PM) emissions. However, primary PM emissions are typically lower than for diesel exhaust.

There is currently a debate of the relative proportions of gasoline and diesel exhaust SOA production in the atmosphere. In a recent study in the Los Angeles, California Basin, Bahreini et al. (2012) noted that diesel consumption was roughly halved on weekends and they found a corresponding reduction in primary organic aerosol (POA) and NO_x but no decrease in SOA that originated from fossil fuel combustion. They concluded that gasoline exhaust is the main source of fossil SOA in the Los Angeles Basin. This suggests that diesel exhaust may dominate the emissions of soot particles in urban areas and gasoline exhaust may dominate the SOA formation. On the contrary, Gentner et al. (2012) characterized the organic aerosol formation potential of emissions from diesel and gasoline vehicles, they concluded that diesel vehicles are responsible for the majority of vehicle SOA but recognized both sources as important. Thus there is a need for more studies especially on the gasoline SOA properties and production rates. Gasoline SOA may also be an important contributor to the early stages of atmospheric transformation of diesel soot. Aging of soot agglomerates strongly alters the optical and hygroscopic properties of soot particles (Zhang et al., 2008; Pagels et al., 2009a).

Odum et al. (1997) investigated the SOA formation from vaporized gasoline and a large number of light aromatic hydrocarbons occurring in reformulated gasoline. They showed that the SOA formation from vaporized whole gasoline can be well approximated by the sum of the SOA formed from the single light aromatic precursors. However, the composition of real-world gasoline exhaust differs from that of vaporized gasoline. For example, the fraction of light aromatics was found to be 21 % by mass in vaporized un-combusted gasoline and 13 % by mass in gasoline exhaust (Schauer et al., 2002). Important classes of compounds with relevance for SOA formation present in gasoline exhaust but not in vaporized gasoline are aldehydes and the complex unresolved mixture of IVOCs not quantified with the gas chromatography – mass spectrometry (GC-MS) techniques typically used (Schauer et al., 2002). Finally, benzene and naphthalene are enriched in the exhaust relative to the fuel (Elghawi et al., 2010).

Kleindienst et al. (2002) performed smog chamber experiments using a gasoline exhaust surrogate mixture made from gasoline fuel and organic additives relevant for the gasoline exhaust. From filter based techniques they concluded that 75–85 % of the SOA could be explained by C_6–C_9 light aromatic compounds and suggested that the remaining fraction was due to higher order aromatics and cyclic and long chain alkenes.

There is a need for investigations of the role of C_6–C_9 light aromatics and additional precursors have in the formation of gasoline SOA in real-world vehicles, particularly in the early aging of gasoline exhaust where IVOCs may be of importance, as has been found for diesel generators (Weitkamp et al., 2007) and wood smoke (Grieshop et al., 2009). There is also a need to define source signatures of gasoline SOA for example in terms of high resolution aerosol mass spectra that can be used for source apportionments studies in ambient air.

In this study, SOA formation of gasoline exhaust emissions from in-use Euro II, Euro III and Euro IV passenger vehicles was investigated in a smog chamber set-up. The aim of this study was: (1) to determine the fraction of the SOA from gasoline exhaust that can be explained by classical C_6–C_9 light aromatics precursors and (2) to investigate whether the chemical composition of the secondary aerosol from gasoline vehicle exhaust can be simulated using only light aromatic precursors. Better understanding of the magnitude and chemical composition of SOA from anthropogenic sources, like gasoline vehicles, will give valuable information to climate modelers and also improve the knowledge of health risks that are linked with air pollution in urban environments.

2 Methods

2.1 Experimental setup

The photo-oxidation experiments were carried out in a 6 m^3 ($W \times L \times H$, $2.1 \times 1.5 \times 1.8$ m) DuPont fluorinated ethylene propylene (FEP) Teflon chamber (Welch Fluorocarbon, USA), with a wall thickness of 125 µm, a smog chamber setup of similar size is presented in Miracolo et al. (2010). For sampling and air exchange three of the vertical sides were each equipped with three 1/4″ and one 3/4″ Kynar fittings. The Teflon chamber was suspended inside a 22 m^3 air conditioned steel chamber. The steel chamber has been described previously by Pagels et al. (2009b).

Four banks positioned on opposite sides of the smog chamber, each consisting of five 100 W fluorescent blacklights (Cleo performance 100-R, Phillips, Netherlands) were used to simulate the spectrum of the UV-band in solar irradiation. The light spectrum ranged from 320 nm to 380 nm, peaking at about 350 nm, which is similar to spectra from several other smog chamber setups (Carter et al., 2005; Presto et al., 2005). The UV spectrum is shown in Fig. S1 in the Supplement. The transmission of FEP at wavelengths between 290 and 800 nm has been reported to be more than 90 % (Paulsen et al., 2005). To enhance the radiation uniformity and intensity in the chamber, the walls of the enclosing steel chamber were coated with reflective aluminum foil. The NO_2-photolysis rate during these experiments was determined to 0.2 min^{-1}, by irradiating a mixture of NO_2 and O_3.

The temperature inside the steel chamber was controlled by a water based cooling unit (model 602D 9.43 kW, CIAT, France). This unit gave the means to control the temperature at 22 °C with a stability of ±2 °C. The temperature was monitored at the midpoint of the Teflon chamber as well as in the space between the smog chamber and the outer steel chamber. A schematic representation of the smog chamber setup and inlet system is shown in Fig. 1.

Gasoline exhaust was injected to the smog chamber through a heated inlet system using an ejector diluter (DI-1000, Dekati Ltd Finland) with an inlet nozzle modified to achieve a primary dilution ratio of 4–5. The ejector was supplied with pressurized air that was preheated to 140 °C and filtered by gas absorbing (NO_x, SO_x, O_3, organic acids) pellets (Triple blend makeup air media, Purafil, USA) and multiple sets of activated carbon and nano particle filters (CLEARPOINT®, Beko, Germany). This filter configuration was used for all pressurized air applications to the chamber. The heated exhaust inlet system and cleaning and conditioning of the smog chamber are further described in the Supplement.

Before each experiment the particle number concentration was $< 100\,\text{cm}^{-3}$ and the particle volume concentration was $< 0.1\,\mu\text{m}^3\,\text{cm}^{-3}$. Blank UV exposure experiments where filtered air was passed through the heated inlet with no exhaust or precursors added to the chamber were performed to make sure that the cleaning procedure worked properly. The formation of secondary organic aerosol was $< 0.1\,\mu\text{g}\,\text{m}^{-3}$ and the formation of nitrate $< 0.01\,\mu\text{g}\,\text{m}^{-3}$ during a typical 2 h blank experiment.

The pressure difference between the inside of the smog chamber and the surrounding steel chamber was monitored by a differential pressure sensor (ASP1400, Sensirion, Switzerland), to ensure that an overpressure was maintained and leaks into the chamber were avoided. The scanning mobility particle sizer (SMPS) data, NO, NO_2, O_3, CO, chamber RH, temperature and differential pressure were logged using a custom made LabVIEW™ (National Instruments, USA) program.

2.2 Vehicles

Three gasoline powered passenger vehicles were used in this study, one Euro II, one Euro III and one Euro IV vehicle, see Supplement Table S1 for more information about the vehicles. All vehicles were driven in normal use in between the experiments. The vehicles were fueled with Swedish standard MK1 gasoline fuel with an octane rating of 95 (“sulfur free” $< 10\,\text{mg}\,\text{kg}^{-1}$). The fuel composition was analyzed with Gas Chromatography-Mass Spectrometry (GC-MS) in a similar way to the exhaust VOC samples as described in Sect. 2.3.3. The mass fraction of C_6–C_9 light aromatics was 30 %. The major oxidative additives used in this fuel were ethanol (5 % by volume) and MTBE 1.2 % by weight. The result of the fuel analysis is given in Table S3.

2.3 Instrumentation

2.3.1 Particle characterization instruments

A custom built SMPS-system (Löndahl et al., 2008) consisting of a Vienna-type (L = 0.28 m, R_1 = 0.025 m, R_2 = 0.0335 m) differential mobility analyzer (DMA) and a condensation particle counter (CPC model 3010, TSI Inc., USA), was used to monitor the size resolved number concentrations. A sheath flow/aerosol flow relationship of 4.9/0.7 $\mathrm{dm^3\,min^{-1}}$ was used for the measurements and the used size range was 10 to 600 nm. The particle volume concentration determined from the SMPS data was used as the volume standard and as a reference value for determination of the collection efficiency of the aerosol mass spectrometer (AMS). The SMPS and AMS were size calibrated with polystyrene latex (PSL)-spheres (80, 100, 240 and 350 nm, Duke Scientific Corp., USA) during the campaign.

The particle chemical composition was measured online by means of a High-Resolution Time of Flight Aerosol Mass Spectrometer (HR-ToF-AMS, Aerodyne research Inc., USA). The instrument was equipped with a laser vaporizer to allow detection of refractory black carbon (rBC; soot), a configuration known as the Soot-Particle Aerosol Mass Spectrometer (SP-AMS). The HR-ToF AMS and SP-AMS are described in detail elsewhere (DeCarlo et al., 2006; Onasch et al., 2012) and briefly below. The aerosol is sampled through an aerodynamic lens, which focuses sub-micrometer particles into a tight beam. The particle beam is modulated to obtain particle size resolved information using the Particle Time of Flight (PToF) mode. After impaction on a heated (600 °C) tungsten vaporizer plate, under low pressure (~ 10 µPa), the operationally defined non-refractory particulate mass (NR-PM) is vaporized and ionized using electron ionization (70 eV). The ions are subsequently analyzed though time of flight mass spectrometry. In these experiments NR-PM is expected to include all PM components except rBC. The instrument was operated in dual vaporizer mode, i.e. both laser and tungsten vaporizers were present. The laser vaporizer was turned on in 5 min periods every hour in most experiments, in order to probe rBC without interfering significantly with the tungsten vaporizer data set. Data analysis was performed with IGOR pro 6 (Wavemetrics, USA), SQUIRREL 1.51 and PIKA 1.1. Elemental analysis (EA) was performed on V-mode data. The fragmentation pattern and calibration factors suggested by Aiken et al. (2008) were used. Nitrate fragments were excluded from the elemental analysis.

2.3.2 Measurement of inorganic gases

The O_3 concentration was monitored using a UV spectrophotometer (model 49i ozone analyzer, Thermo Scientific, USA). The NO and NO_2 (NO_y–NO) concentrations were monitored by a NO_x-monitor (model CLD 700 AL, Eco Physics, USA). The NO_x-instrument uses two measurement chambers which gives a direct measurement of NO and an indirect NO_2 measurement. The principle for measurement of NO_2 is converting NO_2 to NO by a molybdenum converter at high temperature (375 °C); the converter may also convert peroxy acyl nitrates (PAN) and nitric acid (HNO_3) to NO. This gives an interference of the NO_2 signal (Gerboles et al., 2003). The monitoring of O_3 and NO_x were continuous throughout the experiment.

CO, NO_x and O_2 were measured in the raw exhaust by a gas analyzer (model 350 XL, Testo, Germany) in selected experiments. The CO mixing ratio in the smog chamber was typically below 1 ppm for the cold idling experiments and about 8 ppm in the cold start experiment.

2.3.3 Measurement of organic gas-phase compounds

The concentration of light aromatic compounds and other selected VOCs were monitored using a Proton Transfer Reaction Mass Spectrometer (PTR-MS, Ionicon Analytik GmbH, Austria), which allows real time measurements of concentrations down to the ppt range. Since the quadrupole version of the PTR-MS instrument measures only with a unity resolution, different compounds with same nominal mass cannot be distinguished. A detailed description of the PTR-MS technique is given by (Lindinger et al., 1998; de Gouw and Warneke, 2007). The used volume mixing ratio calculations and calibration procedures are described by Taipale et al. (2008).

VOC samples were collected on adsorbent tubes filled with Tenax-TA and Carbopack-B and were analyzed in the laboratory with GC-MS, using a thermal desorption instrument (Perkin-Elmer TurboMatrix 650, Waltham, USA) attached to a gas-chromatograph (Perkin-Elmer Clarus 600, Waltham, USA) with DB-5MS (60 m, 0.25 mm, 1 µm) column and a mass selective detector (Perkin-Elmer Clarus 600T, Waltham, USA). Typically, duplicate adsorbent tube samples were collected before the UV-lights were turned on and at the end of the experiment. Thirteen C_6–C_9 light aromatic compounds and selected alkanes were quantified.

GC-MS was the standard method for determining the mass concentration of C_6–C_9 light aromatic hydrocarbons. The PTR-MS was available in four experiments (I1, I2, S1 and P1) and was used for monitoring of time resolved VOC concentrations. The VOC levels showed good agreement between the methods, see Supplement for comparison Fig. S3.

Initial C_{10}, C_{11} light aromatics and naphthalene concentrations were estimated from the PTR-MS channels m/z 135, 149 and 129 respectively in experiments when the PTR-MS was available, similar measurements have previously been performed by Jobson et al. (2010).

Cumulative OH exposures were estimated to allow investigation of the effect of processing on the aerosol MS composition data. The decay curves of C_8 and C_9 aromatics from PTR-MS and 1,2,4 TMB from GC-MS were fitted using a simple model to derive the OH concentration as a function of time. In the case of using the PTR-MS data, average OH reactivities based on the speciated GC-MS data were used.

2.4 Experimental procedure

Before the experiments, the smog chamber was filled with clean dry pressurized air (relative humidity 3–5 %). A nebulized water (Pro Analysi, Merck, Germany) solution of ammonium sulfate (1 g dm^{-3}) (Merck, Germany), was utilized as condensation seeds to collect the formed low vapor pressure reaction products. The nebulizer (Collison type, Topas Gmbh, Germany) was operated by filtered pressurized air (3 bar). The aerosol particles were dried using a silica diffusion drier and passed through a ^{63}Ni bi-polar charger before introduced to the smog chamber. The salt seeds were injected for about 20–30 min until a concentration of 15–20 $\mu g\,m^{-3}$ was accomplished, corresponding to an initial number concentration of 20 000–25 000 particles cm^{-3}.

Two different idling cases were defined: (1) cold start; the vehicle was started on site (after cold soaking for > 3 h) and the exhaust was injected to the smog chamber from first ignition. (2) Cold idling; the vehicles were driven for about 3 min on a standardized circuit before injection, until an engine temperature of $55 \pm 5\,^{\circ}C$ was established. The ambient temperature was between −5 and +3 °C during the campaign (Table S2 Supplement).

In the precursor experiments, *m*-xylene or a mixture of three selected precursors were injected through evaporation from a glass flask purged with pressurized air. The precursors used were: toluene (> 99.5 % Merck, Germany) *m*-xylene (> 99 %, Sigma-Aldrich, USA) and 1,2,4-trimethylbenzene (> 98 %, Alfa Aesar, Germany). 1,2,4-trimethylbenzene was chosen because it is often the most abundant C_9-aromatic in idling gasoline exhaust (Table S3 in Supplement and Schauer et al., 2002).

The target VOC concentration in the chamber for each gasoline exhaust experiment was established using PTR-MS (raw spectrum intensities of m/z 93, 107, 121) sampling from the smog chamber and a flame ionization detector (FID, Model RS 53-T, Ratfisch, Germany), sampling from the raw exhaust. The total VOC concentration (FID) was between 1 and 2.5 ppm in the gasoline exhaust experiments. The length of the exhaust injection period was typically 5–15 min for cold idling and 60 s for cold start. Including the dilution in the Teflon chamber a total dilution ratio for the cold idling experiments of 30–120 was achieved, depending on the injection time of the exhaust. Additional NO typically had to be added after the exhaust injection to achieve a desired ratio between light aromatics (LA) and NO_x (ppbC/ppb). In four gasoline exhaust experiments and the two precursor experiments (Table 2) a light aromatic to NO_x ratio of around 50 was used. In experiments I3 and I4 lower LA to NO_x ratios of 13 and 7, respectively were used. In experiment I4 O_3 was added to convert a major fraction of the emitted NO into NO_2. The level of NO at the start of the experiments was 35–107 ppb. O_3 was produced by a modified spark discharge ozone generator (AM 3000-2, Ozone Technology, Sweden) using pure O_2 (medical grade, Air Liquid).

After exhaust injection and addition of NO or O_3 there was a period of 30 to 60 min to allow mixing in the chamber and for characterization of the fresh exhaust composition. After this the UV-lights were lit, which is referred to as time $t = 0$ throughout the paper. The length of the experiments was 3–4 h.

2.5 Data analysis

2.5.1 Wall loss corrections

Aerosol particles suspended in a Teflon chamber may deposit to the chamber walls (McMurry and Rader, 1985), due to electrostatic forces and other deposition mechanisms, such as sedimentation and diffusion. To be able to quantify the SOA formation, wall losses have to be accounted for. In this work, a wall loss correction method based on AMS data was used (Hildebrandt et al., 2009). An assumption is made that VOCs do not condense on the chamber walls but are rather in equilibrium with particles deposited on the walls. The particulate sulfate seed is then conserved by the chamber system. The organic aerosol mass concentration ($C_{OA}(t)$) as a function of time is calculated by Eq. (1), by multiplying the mass concentration of seed aerosol at the time when UV-light was initiated ($C_{seed}^{sus}(t = 0)$) with the ratio between organic aerosol ($C_{OA}^{sus}(t)$) and ammonium sulfate seed concentrations ($C_{seed}^{sus}(t)$) derived from AMS-data. $C_{seed}^{sus}(t = 0)$ is derived from SMPS measurements, using a ρ_{seed} of 1.769 g cm^{-3}.

$$C_{OA}(t) = \frac{C_{OA}^{sus}(t)}{C_{seed}^{sus}(t)} C_{seed}^{sus}(t = 0) \qquad (1)$$

Secondary sulfates may also form in the chamber from oxidation of SO_2. However, the sulfur content of European gasoline fuel is extremely low ($< 10\,\mathrm{mg\,kg^{-1}}$). To make sure that secondary sulfates did not bias the measurements, we carried out several nucleation experiments with gasoline exhaust under conditions similar to the seeded experiments. It was found that secondary sulfate formation was 0.1–0.3 $\mu\mathrm{g\,m^{-3}}$. The resulting influence of the wall loss corrected SOA concentration is therefore less than 5 % in every experiment.

The half-life of ammonium sulfate mass concentration in experiments with no or negligible SOA formation was found to be ~ 3 h for the period starting when the UV-lights were turned on, which makes quantitative experiments meaningful up to about 4 h after UV on.

2.5.2 Aerosol mass yield

The aerosol mass yield Y at time $= t$ is defined as the ratio between the wall-loss corrected formed organic mass concentration divided by the mass concentration of reacted VOCs (ΔHC), at time $= t$ (Eq. 2) (Odum et al., 1997).

$$Y = \frac{C_{\mathrm{SOA}}}{\Delta \mathrm{HC}} \tag{2}$$

In the calculations presented in this paper t exclusively refers to the end of the experiment. For the gasoline experiments an apparent mass yield was calculated taking into account only C_6–C_9 alkyl substituted light aromatics and benzene, thus the ΔHC term only consists of these compounds. These apparent mass yields can then be compared with true mass yields from the pure precursor experiments carried out at similar conditions in our chamber, to gain insight into the fraction of formed SOA that originated from C_6–C_9 light aromatics.

2.5.3 Primary exhaust particles and subtraction of primary organic aerosol

Upon exhaust injection an immediate increase in OA was observed in each experiment, after which a plateau was reached. This fraction of OA is referred to as Primary Organic Aerosol (POA). The ratio of POA to sulfate seed was assumed to be constant throughout the experiments. The estimated POA concentration at the end of the experiment was subtracted from the wall-loss corrected organic concentrations to determine C_{SOA}. The POA and particulate nitrates observed in these experiments will be treated in more detail in future publications.

The primary emissions from the Euro II vehicle were investigated in a separate experiment without condensation seeds. The emissions of primary particles were less than 50 particles cm^{-3} in the smog chamber at a dilution ratio of 1 : 36 for the cold idling gasoline emissions, indicating that the concentration of primary particles (such as soot cores) were negligible compared to the seed aerosol ($\sim$ 20 000–25 000 cm^{-3}). Only in the cold start experiment (S1), there was a noticeable increase in the number concentration (about 2000 cm^{-3}) upon adding the exhaust to the chamber. Similarly, only in the cold start experiment there was a noticeable signal of rBC (soot) detected with the SP-AMS. The mass concentration of rBC was estimated to 1.5 µg m^{-3} and < 0.3 µg m^{-3} in the cold start and cold idling experiments, respectively.

3 Results and discussion

A summary of the results and conditions from six gasoline exhaust experiments and two precursor experiments is presented in Table 2. Photo-oxidation of gaseous gasoline exhaust forms SOA and ammonium nitrate. At the end of the experiments the formed SOA is 9–500 times higher than the emitted POA, which is in sharp contrast to diesel exhaust where the contribution of primary PM often dominates over secondary PM (Chirico et al., 2010). Experiment I1 had the highest contribution of POA corresponding to 12 % of the OA in the chamber at the end of the photo-oxidation experiment, while in experiments I2 and I3 the POA contribution was less than 0.5 %. The POA most likely originates from organic compounds with volatility low enough to condense onto the seed particles when the exhaust is cooled down after injection in the smog chamber. The aerosol mass spectra of these primary emissions were similar to diesel exhaust POA and the hydrocarbon-like organic aerosol (HOA) found in urban areas.

3.1 VOC composition and emissions

The classical light aromatic precursors (C_6–C_9) constituted 30 % of the fuel by mass but only 10–15 % of the total VOC emissions in the gasoline exhaust, where the latter figure includes methane (Table 1).

In Fig. 2 it is shown that the distribution of light aromatic SOA precursors depends on both vehicle type and operation mode. In the cold start with the Euro IV vehicle, the distribution of the light aromatics is similar to the distribution in the fuel. In the cold start experiment it is expected that the VOC-emissions may be well represented by vaporized fuel, due to the low temperatures of the engine and the oxidation catalyst (Schifter et al., 2010). A more detailed analysis of the light aromatic content in the fuel and gasoline exhaust is presented in Table S3 in the Supplement.

The distribution of light aromatics from the Euro II vehicle was fairly repeatable under cold idling conditions (Fig. 2) and shows an even distribution between the C_6–C_9 light aromatics. The Euro III and Euro IV vehicles when used under cold idling showed a trend towards decreasing concentration with increasing molecular size. The benzene concentration is strongly elevated in these cold idling experiments compared to the fuel content (benzene is regulated to < 1 % by volume in gasoline in Europe), most likely due to formation of benzene from other light aromatic compounds in the catalyst (Bruehlmann et al., 2007). The enrichment of benzene in the exhaust is also found in road tunnel emission measurements (Legreid et al., 2007). The distribution of light aromatics from the cold idling case reasonably well represents the road tunnel data.

The concentration of C_{10} and C_{11} light aromatics and naphthalene were assessed from the corresponding PTR-MS channels: $m/z = 135$, 149 and 129. This was done for the Euro II vehicle at cold idling (I1 and I2 experiments) and the cold start experiment (S1) with the Euro IV vehicle. The contribution in percent to the summed initial mixing ratio (ppb) of C_6–C_{11} light aromatics and naphthalene was as follows 4.6; 0.4 % (C10), 0.8; < 0.1 % (C11) and 1.1; < 0.1 % (naphthalene) for cold idling (I1 and I2) and cold start respectively. As it can be seen the C_{10}, C_{11} and naphthalene fraction is significantly higher at cold idling compared to the cold start.

3.2 Formation of gasoline SOA

Figure 3a, b compares the temporal evolution for one representative gasoline experiment (I2) and an experiment with a precursor mixture (P1) containing three of the most important C_7–C_9 light aromatic precursors. The upper panels show the mixing ratios of NO, NO_2 and O_3 (left y-axis) and the ratio of nitrate and OA to sulfate seed (right y-axis). The middle panels show the mixing ratios for the most important light aromatic precursors and one photochemical gas-phase reaction product, obtained by PTR-MS. The PTR-MS channels correspond to toluene (C_7 $m/z = 93$), C_8 ($m/z = 107$), C_9 ($m/z = 121$), C_{10} ($m/z = 135$) aromatics and acetaldehyde ($m/z = 45$). In the P1 experiment (Fig. 3b) toluene, *m*-xylene (C_8) and 1,2,4 trimethylbenzene (C_9) were used as precursors. The lower panels show the H : C and O : C elemental ratios of the formed SOA, derived from AMS data.

The SOA formation is delayed 30–45 min after the lights are turned on corresponding to the time required to initiate photochemistry and for NO to be converted to NO_2 (Fig. 3). The NO to NO_2 conversion, and thereby the formation of ozone and HO_x occurs slightly faster in the gasoline exhaust experiment compared to the pure precursor experiment. The delay between ozone and SOA formation is shorter and the SOA formation starts at a higher NO level in the idling gasoline exhaust experiment compared to the precursor experiment. These differences are attributed to the large group of additional VOCs (in addition to C_6–C_9 light aromatics) present in the gasoline exhaust compared to the pure precursor experiment.

The initial concentrations of C_7–C_9-aromatics are all at a similar level in the cold idling gasoline exhaust, while the C_{10}-aromatics are present in much lower concentrations. The reactivity typically increases with increasing carbon number. For example *m*-xylene and 1,2,4-trimethylbenzene are much more reactive than toluene. The sum of the concentration of reacted light aromatics (C_6–C_9) is used for mass yield calculations, although the reacted fraction of benzene is small under the prevailing (atmospherically relevant) OH-radical concentrations ($1–3 \times 10^6\,\mathrm{cm}^{-3}$), due to its low reactivity with the OH-radical.

The O : C and H : C ratios were both similar for the gasoline exhaust and the precursor experiment (∼ 0.4 and ∼ 1.4, respectively). Figure 4 shows the wall loss corrected mass concentration of SOA, nitrate and excess ammonium for experiment I2 (a), I3 (b) and P1 (c), the ammonium sulfate seed mass has been subtracted. The reacted mass concentration of C_6–C_9 light aromatics were about two times higher for the precursor experiment compared to the gasoline exhaust experiments. Still, the wall loss corrected SOA mass concentration was similar (Table 2).

Formation of nitrate occurs only to a limited extent in the precursor experiments (about 4 % of the total organics). The nitrate formation in the precursor experiment is attributed to formation of particle phase organic nitrates, while the formation of nitrate in the gasoline experiments can be attributed to a mixture of ammonium nitrate and organic nitrates that varies strongly between experiments. Information on the occurrence of organic and ammonium nitrate can be obtained from the NO / NO_2 ion fragment ratio in the AMS. The NO / NO_2 ratio is substantially higher for SOA from light aromatic precursors compared to ammonium nitrate (Sato et al., 2010). This analysis will be reported separately.

The ammonium nitrate is most likely formed by reactions of ammonia from the car exhaust and HNO_3 formed by reactions in the smog chamber (originating from NO_x). SOA from passenger vehicle emissions co-condenses with ammonia and nitric acid as can be expected during atmospheric processing of pollutants. The ammonium nitrate formation increased with increasing initial NO_x level and thus in experiment I3 the aerosol was dominated by nitrate.

3.3 Mass yield of gasoline exhaust and precursors

The apparent mass yield, Y is defined here as the ratio between the mass concentration of formed secondary organic aerosol, C_{SOA} and the mass concentration of reacted light aromatic compounds (C_6–C_9), ΔHC (Eq. 2). By comparing the apparent mass yields with the yields from the precursor experiments at a given C_{SOA} we can infer the contribution from additional SOA precursors. The apparent mass yield from C_6–C_9 light aromatics in the gasoline exhaust SOA increases with increasing concentration of organic aerosol in the smog chamber as has been shown in several previous studies for yields of single precursor systems (Cocker et al., 2001; Song et al., 2005; Ng et al., 2007; Hildebrandt et al., 2009). A two-product fit (Odum et al., 1997) to the cold idling data is shown in Fig. 5.

Our precursor data agree well with *m*-xylene data from Song et al. (2005) carried out at similar conditions (so called classical photo-oxidation experiments), therefore we used their fit to extend the comparison between our precursor and gasoline exhaust data towards lower mass concentrations. The mass yield for experiment P1 and P2 is lower than some pure precursor experiment presented in the literature (Hildebrandt et al., 2009; Ng et al., 2007). Those experiments with significantly higher yield were often performed in the "low-NO_x regime" using H_2O_2 as OH-precursor. The experiments presented in this paper were performed without added OH-precursors and do all start in the "high NO_x regime" and as the NO concentration goes towards zero the experiment moves towards the "low NO_x regime". The VOCs which reacted in the "high NO_x" regime, are likely to form products that is too volatile to end up in the particle phase, when oxidized at the OH radial concentration used here (Ng et al., 2007).

According to the fits, the apparent mass yield of the gasoline exhaust from intermediate idling is about 1.7 times higher than the yield of the pure precursors under the conditions in this study. Thus, about 1.7 times more C_6–C_9 light aromatics have been reacted in the precursor experiments to form the same mass concentration of SOA (Eq. 2). If we assume that the reacted C_6–C_9 aromatic precursors form the same amount of SOA in the complex mixture in the gasoline exhaust as they do in the pure precursor experiments this would indicate that about 60 % of the SOA in the gasoline exhaust originates from C_6–C_9 precursors and 40 % from additional precursors (Fig. 5). The cold start experiment was an exception as it falls essentially on the fit of the yield of pure precursors.

By percentage, the reacted light aromatic compounds in the cold idling gasoline exhaust were on average 0.9 % benzene, 9.3 % toluene, 29.1 % C_8, 41.5 % C_9, 17.2 % C_{10}, and 2.0 % C_{11}. Assuming that the C_{10} and C_{11} light aromatics have similar yields as the C_8–C_9 aromatics, C_{10} and C_{11} aromatics would be responsible for about 11 % and 1 % respectively of the SOA formed. Additional candidates as SOA precursors will be discussed in Sect. 3.4.

The fraction of emitted C_{10} and C_{11} light aromatics and naphthalene were all substantially lower in the cold start experiment which is consistent with the classical C_6–C_9 aromatics being responsible for a larger fraction of the formed SOA in this case. Thus, SOA-formation from cold start emissions but not from cold idling could be well described by only including the C_6–C_9 light aromatics.

3.4 Chemical composition

High-resolution SOA mass spectra from experiment I2 and P1 are shown in Fig. 6. The AMS ion fragments have been grouped into four families based on their carbon, hydrogen and oxygen content. The dominating organic m/z peaks in SOA from gasoline exhaust are m/z 44 followed by m/z 43 (Fig. 6a), while the reverse trend was found in the precursor experiments (Fig. 6b).

The peaks at m/z 43 and 44 were dominated by $C_2H_3O^+$ and CO_2^+ fragments respectively, for both the gasoline exhaust and the precursor experiments. These two are the most abundant fragments in ambient oxygenated organic aerosol (OOA). CO_2^+ is typically the main fragment for low volatility OOA (LV-OOA) while in semi-volatile OOA (SV-OOA) CO_2^+ and $C_2H_3O^+$ are of similar magnitude (Ng et al., 2010).

The gasoline SOA mass spectrum (Fig. 6a) shows strong similarities to atmospheric observations of fresh OOA detected in and downwind urban areas and gasoline SOA may thus be an important contributor to SOA in these locations as recently hypothesized from ambient data (Bahreini et al., 2012). Although SOA from many different sources show similarities, a few differences compared to diesel exhaust SOA should be pointed out. For example, diesel SOA (Chirico et al., 2010) has significant contributions from hydrocarbon fragments in the C_nH_{2n+1} series (for example $C_3H_7^+$ and $C_4H_9^+$). The main hydrocarbon fragments in the gasoline SOA are instead $C_3H_3^+$ and $C_3H_5^+$ consistent with aromatic (and potentially also alkene) precursors that have a H/C ratio closer to 1.

The organic mass fraction detected at m/z 43 ($f43$) and m/z 44 ($f44$) from the AMS measurements at the end of each experiment is shown in Fig. 7a. The figure also features the triangular boundary of atmospheric OOA observations introduced by Ng et al. (2010). Photochemical aging in the atmosphere typically increases the $f44$ in the organic spectra; a relatively high $f44$ indicates that the atmospheric aging process is more progressed.

The concept of the triangular space is formulated for atmospheric measurements of aged aerosols from multiple precursors and sources. Since gasoline exhaust SOA is a more complex mixture than SOA from pure precursors, it can be expected that gasoline SOA resembles atmospheric observations better than SOA from pure precursors. It is also apparent that SOA from a relevant mixture of light aromatics are not able to adequately simulate the composition of the SOA from early ageing of gasoline exhaust.

For one cold idling and one precursor experiment we have plotted the $f43$ vs. $f44$ relationship as a function of cumulative OH exposure. A cumulative OH exposure of $9 \times 10^6\,cm^{-3}\,h$ corresponds to 9 h of aging at a 24 h mean OH concentration of $1 \times 10^6\,cm^{-3}$. For the cold idling experiment there is an increase in both $f43$ and $f44$ with increasing OH exposure, while for the precursor mixture the *f*43, *f*44 relationship is little influenced.

A van Krevelen diagram, showing the hydrogen to carbon (H : C) and oxygen to carbon (O : C) ratios is shown in Fig. 7b. The diagram depicts the molar ratios at the end of each experiment. The H : C ratio varies between 1.2 and 1.55 and the O : C ratio 0.36 to 0.43 for the set of experiments and there is no systematic difference between gasoline exhaust and pure precursor experiments in this aspect. A higher O : C and lower H : C ratio represents a higher oxidation state. Average carbon oxidation (OS_C) states can be estimated from O : C and H : C (Kroll et al., 2011). The SOA produced in these experiments have OS_C ranging from −0.8 to −0.4, similar to SV-OOA in the atmosphere. The diagonal red lines indicate oxidation states −1, −0.5 and 0.

An important observation is that the cold idling gasoline exhaust and pure precursor experiments are clearly separated in terms of their *f*43/*f*44 relationship but not in terms of their O : C vs H : C relationship and the division of ions into four different families dependent on their composition. This is not contradictory since m/z 44 and 43 only represent a fraction of the organic MS while the atomic ratios are calculated from the full spectra. A higher abundance of $C_2H_3O^+$ (the main fragment at m/z 43 in these data) pulls the O : C ratio towards 0.5 and the H : C ratio towards 1.5. The remaining fraction of the precursor SOA MS compensates this effect.

The *f*43, *f*44 values from this study are compared with literature data for light aromatic precursors in Fig. 8. The precursor experiments reported here are in general agreement with previous studies of SOA from pure *m*-xylene and 1,3,5-TMB (Ng et al., 2010) both positioned to the right of the triangular plot.

From known literature values of the fragmentation patterns of the dominating C_6–C_9 light aromatic compounds we calculated the theoretically expected fragmentation pattern of the gasoline exhaust assuming that only the C_6–C_9 light aromatic compounds were contributing to the SOA. It was assumed that the fragmentation pattern of the mixed SOA could be determined as the weighted sum of the fragmentation patterns of

SOA from the individual precursors. The procedure and the in-data to this calculation are shown in more detail in the Supplement.

It is found (Fig. 8.) that the expected $f43$ calculated, as described above, is slightly lower for the actual gasoline exhaust experiments than for the pure precursor experiments, but still substantially higher than that experimentally found in the cold idling experiments. The small difference compared to the three component precursor mixture used in our experiment is due to the low $f43$ of ethyl benzene and slightly higher toluene content in the gasoline exhaust compared to experiment P1. From this analysis we can put constraints on the magnitude and composition of SOA from the additional precursors discussed above.

If we subtract the expected $f43$ and $f44$ fractions based on only C_6–C_9 aromatics from the mass spectra at the end of each gasoline exhaust experiment, it can be shown that a maximum 50–60 % of the mass would come from light aromatics, (S4 in the Supplement). At higher fractions of light aromatic precursors, the $f43$ fraction of the unknown additional precursors would become below 0. In contrast, for the cold start experiment, the $f43/f44$ relationship assuming only C_6–C_9 precursors is almost identical to the experimentally found value, again supporting that the cold start emissions can be explained from essentially C_6 to C_9 light aromatics only.

This indicates that the additional precursors are likely to produce SOA with low $f43$, to the left of the triangle in Fig. 8. Possible precursors for the non-light aromatic SOA that do produce SOA with low $f43$ are 2-ring PAHs such as naphthalene (Fig. 8), which has been identified as an important SOA precursor in aging of diesel exhaust (Chan et al., 2009).

Naphthalene have also previously been quantified in gasoline exhaust at similar proportions compared to the sum of C_6–C_9 light aromatics (Schauer et al., 2002) as was found in the cold idling experiments here. The mass yield from two-ring PAHs in low-NO_x and high-NO_x photooxidation experiments (Chan et al., 2009) is about two and four times greater respectively, than the mass yield from similar experiments (Ng et al.,

2007) with *m*-xylene as precursor. This implies that relatively low concentrations of PAHs can give a significant contribution to SOA formation.

We used our measured initial naphthalene concentration and the known OH reactivity to estimate the reacted concentration of naphthalene, and assumed that the mass yield for naphthalene is three times higher than the yield for *m*-xylene in our chamber under the conditions studied. We found that naphthalene could contribute with around 5 % of the SOA mass in experiment I1 and I2. Results from Schauer et al. (2002) suggested that the summed concentration of 1- and 2-methyl naphthalene could be up to 150 % of the naphthalene concentration in gasoline exhaust, but those were not measured in our experiments. If and when methyl-naphthalenes are present in such significant concentrations, they would have to be considered as important SOA precursors in the early aging of gasoline exhaust due to their high yield and OH-reactivity (Chan et al., 2009). The result of superposition of SOA from light aromatic and naphthalene precursors in the "Ng-triangle" would decrease the discrepancy in composition between expected and measured values for gasoline exhaust.

As discussed above, we also estimated that C_{10} and C_{11} aromatics could contribute to about 12 % of the SOA in experiment I1 and I2. If the experiments would have proceeded to a higher cumulative OH exposure it is likely that a larger fraction of the formed SOA would originate from C_6 to C_9 aromatics, since they occur in higher concentration but have a lower OH-reactivity than the larger aromatic molecules, The shift towards higher $f43$ and $f44$ with increasing cumulative OH exposure shown for experiment I3 is consistent with naphthalenes being a major contributor in the early phase of SOA formation in gasoline exhaust.

In addition to the C_{10} and C_{11} light aromatics and naphthalenes a minor part of the remaining SOA may possibly be formed by other IVOCs such as phenols (that also produce low $f43$ SOA Chhabra et al., 2011), aromatic aldehydes, long chain and branched alkanes and alkenes and highly reactive compounds (such as styrene). Finally, an additional potentially important effect could be that photo-oxidation of light aromatics in a more complex mixture, like gasoline exhaust, results in more complex reaction products and SOA with different composition, and an altered SOA yield compared to pure precursor experiments (Song et al., 2007).

3.5 SOA production factors

SOA production factors (PF) ($\mathrm{g\,kg^{-1}}$) are calculated using Eq. (3), where the numerator is the SOA concentration ($\mathrm{\mu g\,m^{-3}}$) and the denominator is the concentration of total combusted carbon ($\mathrm{\mu g\,m^{-3}}$). ω_c is the carbon content in fuel which is 0.85 (Kirchstetter et al., 1999). HC is the total hydrocarbons in the raw exhaust, BC is the black carbon emitted and we assume that all organic carbon is emitted in gas phase.

$$\mathrm{PF} = 10^3\left([\mathrm{SOA}]/([\mathrm{CO_2}]+[\mathrm{CO}]+[\mathrm{HC}]+[\mathrm{BC}])\right)\omega_c \qquad (3)$$

The SOA production factors ranged between 0.005 and 0.09 $\mathrm{g\,kg^{-1}}$ for the cold idling experiments, the PF for the cold start experiment was 0.48 $\mathrm{g\,kg^{-1}}$. Compared to emission factors from diesel passenger vehicles reported by Chirico et al. (2010), the PF from the cold start is in the same range as the PF from diesel vehicles with deactivated oxidation catalyst (0.254 to 0.461 $\mathrm{g\,kg^{-1}}$). The PF from cold idling gasoline vehicles is similar to or higher than that for diesel vehicles with functioning catalyst (0.012–0.020 $\mathrm{g\,kg^{-1}}$) (Chirico et al., 2010). Platt et al. (2012) have reported a SOA emission factor of 0.345 for a gasoline vehicle undergoing a complete driving cycle.

4 Conclusions

VOC emissions from gasoline vehicles when the engine and catalyst have not yet reached their operating temperature are substantial. Since the driving pattern in urban environments includes idling and shorter driving stints, which may hinder the engine and catalyst from reaching its optimum operating temperature, gasoline vehicles may significantly contribute to the VOC emissions to urban air. The gasoline fuel and VOC emissions have a substantial contribution of C_6–C_9 light aromatic compounds that are known SOA precursors. As shown in this study gasoline exhaust readily forms secondary organic aerosol with a signature aerosol mass spectrum with similarities to the oxidized organic aerosol that commonly dominates the OA mass spectra in and downwind urban areas. This substantiates recent claims that gasoline SOA is a dominating source to SOA in and downwind large metropolitan areas (Bahreini et al., 2012). Evidence for additional SOA precursors that are responsible for 40 % or more of the formed gasoline SOA during cold idling has been shown using two independent approaches. These were based on (1): the difference in apparent mass yield and (2): the difference in chemical composition between SOA from gasoline exhaust and that of pure precursors. Important candidate contributors are higher order aromatic compounds such as C_{10}, C_{11} light aromatics, naphthalenes and methyl-naphthalenes. In contrast, during a cold start experiment, the distribution of light aromatics was consistent with vaporized fuel and the apparent mass yield and the aerosol mass spectra were both consistent with C_6–C_9 light aromatics being responsible for more than 90 % of the SOA formation.

Supplementary material related to this article is available online at: http://www.atmos-chem-phys-discuss.net/12/31725/2012/ acpd-12-31725-2012-supplement.pdf.

Acknowledgements. This work was supported by the Swedish Research Council for Environment, Agricultural Sciences and Spatial Planning FORMAS through projects 2007-1205, 2008-1467, 2009-615 and 2010-1678, the Swedish Research Council through project 2006-5940 and by Metalund, the centre for Medicine and Technology for Working Life and Society, a competence centre at Lund University, Sweden, supported by FAS, the Swedish Council for Working Life and Social Research.

References

Aiken, A. C., Decarlo, P. F., Kroll, J. H., Worsnop, D. R., Huffman, J. A., Docherty, K. S., Ulbrich, I. M., Mohr, C., Kimmel, J. R., Sueper, D., Sun, Y., Zhang, Q., Trimborn, A., Northway, M., Ziemann, P. J., Canagaratna, M. R., Onasch, T. B., Alfarra, M. R., Prevot, A. S. H., Dommen, J., Duplissy, J., Metzger, A., Baltensperger, U., and Jimenez, J. L.: O/C and OM/OC ratios of primary, secondary, and ambient organic aerosols with high-resolution time-of-flight aerosol mass spectrometry, Environ. Sci. Technol., 42, 4478–4485, 2008.

Bahreini, R., Middlebrook, A. M., de Gouw, J. A., Warneke, C., Trainer, M., Brock, C. A., Stark, H., Brown, S. S., Dube, W. P., Gilman, J. B., Hall, K., Holloway, J. S., Kuster, W. C., Perring, A. E., Prevot, A. S. H., Schwarz, J. P., Spackman, J. R., Szidat, S., Wagner, N. L., Weber, R. J., Zotter, P., and Parrish, D. D.: Gasoline emissions dominate over diesel in formation of secondary organic aerosol mass, Geophys. Res. Lett. 39, L06805, doi:10.1029/2011GL050718, 2012.

Bruehlmann, S., Novak, P., Lienemann, P., Trottmann, M., Gfeller, U., Zwicky, C. N., Bommer, B., Huber, H., Wolfensberger, M., and Heeb, N. V.: Three-way-catalyst induced benzene formation: a precursor study, Appl. Catal. B-Environ. 70, 276–283, 2007.

Carter, W. P. L., Cocker, D. R., Fitz, D. R., Malkina, I. L., Bumiller, K., Sauer, C. G., Pisano, J. T., Bufalino, C., and Song, C.: A new environmental chamber for evaluation of gas-phase chemical mechanisms and secondary aerosol formation, Atmos. Environ. 39, 7768–7788, 2005.

Chan, A. W. H., Kautzman, K. E., Chhabra, P. S., Surratt, J. D., Chan, M. N., Crounse, J. D., Kürten, A., Wennberg, P. O., Flagan, R. C., and Seinfeld, J. H.: Secondary organic aerosol formation from photooxidation of naphthalene and alkylnaphthalenes: implications for oxidation of intermediate volatility organic compounds (IVOCs), Atmos. Chem. Phys., 9, 3049–3060, doi:10.5194/acp-9-3049-2009, 2009.

Chhabra, P. S., Ng, N. L., Canagaratna, M. R., Corrigan, A. L., Russell, L. M., Worsnop, D. R., Flagan, R. C., and Seinfeld, J. H.: Elemental composition and oxidation of chamber organic aerosol, Atmos. Chem. Phys., 11, 8827–8845, doi:10.5194/acp-11-8827-2011, 2011.

Chirico, R., DeCarlo, P. F., Heringa, M. F., Tritscher, T., Richter, R., Prévôt, A. S. H., Dommen, J., Weingartner, E., Wehrle, G., Gysel, M., Laborde, M., and Baltensperger, U.: Impact of aftertreatment devices on primary emissions and secondary organic aerosol formation potential from in-use diesel vehicles: results from smog chamber experiments, Atmos. Chem. Phys., 10, 11545–11563, doi:10.5194/acp-10-11545-2010, 2010.

Cocker, D. R., Mader, B. T., Kalberer, M., Flagan, R. C., and Seinfeld, J. H.: The effect of water on gas-particle partitioning of secondary organic aerosol: II. *m*-xylene and 1,3,5-trimethylbenzene photooxidation systems, Atmos. Environ., 35, 6073–6085, 2001.

de Gouw, J. and Jimenez, J. L.: Organic aerosols in the Earth's Atmosphere, Environ. Sci. Technol., 43, 7614–7618, 2009.

de Gouw, J. and Warneke, C.: Measurements of volatile organic compounds in the earths atmosphere using proton-transfer-reaction mass spectrometry, Mass Spectrom. Rev., 26, 223–257, 2007.

DeCarlo, P. F., Kimmel, J. R., Trimborn, A., Northway, M. J., Jayne, J. T., Aiken, A. C., Gonin, M., Fuhrer, K., Horvath, T., Docherty, K. S., Worsnop, D. R., and Jimenez, J. L.: Field-deployable, high-resolution, time-of-flight aerosol mass spectrometer, Anal. Chem., 78, 8281–8289, 2007.

Elghawi, U. M., Mayouf, A., Tsolakis, A., and Wyszynski, M. L.: Vapour-phase and particulate-bound PAHs profile generated by a (SI/HCCI) engine from a winter grade commercial gasoline fuel, Fuel, 89, 2019–2025, 2010.

Gentner, D. R., Isaacman, G., Worton, D. R., Chan, A. W. H., Dallmann, T. R., Davis, L., Liu, S., Day, D. A., Russell, L. M., Wilson, K. R., Weber, R., Guha, A., Harley, R. A., and Goldstein, A. H.: Elucidating secondary organic aerosol from diesel and gasoline vehicles through detailed characterization of organic carbon emissions, P. Natl. Acad. Sci., 109, 18318–18323, 2012.

Gerboles, M., Lagler, F., Rembges, D., and Brun, C.: Assessment of uncertainty of NO_2 measurements by the chemiluminescence method and discussion of the quality objective of the NO_2 European Directive, J. Environ. Monitor., 5, 529–540, 2003.

Grieshop, A. P., Donahue, N. M., and Robinson, A. L.: Laboratory investigation of photochemical oxidation of organic aerosol from wood fires 2: analysis of aerosol mass spectrometer data, Atmos. Chem. Phys., 9, 2227–2240, doi:10.5194/acp-9-2227-2009, 2009.

Hallquist, M., Wenger, J. C., Baltensperger, U., Rudich, Y., Simpson, D., Claeys, M., Dommen, J., Donahue, N. M., George, C., Goldstein, A. H., Hamilton, J. F., Herrmann, H., Hoffmann, T., Iinuma, Y., Jang, M., Jenkin, M. E., Jimenez, J. L., Kiendler-Scharr, A., Maenhaut, W., McFiggans, G., Mentel, Th. F., Monod, A., Prévôt, A. S. H., Seinfeld, J. H., Surratt, J. D., Szmigielski, R., and Wildt, J.: The formation, properties and impact of secondary organic aerosol: current and emerging issues, Atmos. Chem. Phys., 9, 5155–5236, doi:10.5194/acp-9-5155-2009, 2009.

Heeb, N. V., Forss, A. M., Bruhlmann, S., Luscher, R., Saxer, C. J., and Hug, P.: Three-way catalyst-induced formation of ammonia-velocity- and acceleration-dependent emission factors, Atmos. Environ., 40, 5986–5997, 2006.

Hildebrandt, L., Donahue, N. M., and Pandis, S. N.: High formation of secondary organic aerosol from the photo-oxidation of toluene, Atmos. Chem. Phys., 9, 2973–2986, doi:10.5194/acp-9-2973-2009, 2009.

Jobson, B. T., Volkamer, R. A., Velasco, E., Allwine, G., Westberg, H., Lamb, B. K., Alexander, M. L., Berkowitz, C. M., and Molina, L. T.: Comparison of aromatic hydrocarbon measurements made by PTR-MS, DOAS and GC-FID during the MCMA 2003 Field Experiment, Atmos. Chem. Phys., 10, 1989–2005, doi:10.5194/acp-10-1989-2010, 2010.

Kean, A. J., Littlejohn, D., Ban-Weiss, G. A., Harley, R. A., Kirchstetter, T. W., and Lunden, M. M.: Trends in on-road vehicle emissions of ammonia, Atmos. Environ., 43, 1565–1570, 2009.

Kirchstetter, T. W., Harley, R. A., Kreisberg, N. M., Stolzenburg, M. R., and Hering, S. V.: On-road measurement of fine particle and nitrogen oxide emissions from light- and heavy-duty motor vehicles, Atmos. Environ., 33, 2955–2968, 1999.

Kleindienst, T. E., Corse, E. W., Li, W., McIver, C. D., Conver, T. S., Edney, E. O., Driscoll, D. J., Speer, R. E., Weathers, W. S., and Tejada, S. B.: Secondary organic aerosol formation from the irradiation of simulated automobile exhaust. J. Air Waste Manage., 52, 259–272, 2002.

Kroll, J. H., Donahue, N. M., Jimenez, J. L., Kessler, S. H., Canagaratna, M. R., Wilson, K. R., Altieri, K. E., Mazzoleni, L. R., Wozniak, A. S., Bluhm, H., Mysak, E. R., Smith, J. D., Kolb, C. E., and Worsnop, D. R.: Carbon oxidation state as a metric for describing the chemistry of atmospheric organic aerosol, Nat. Chem., 3, 133–139, 2011.

Legreid, G., Reimann, S., Steinbacher, M., Staehelin, J., Young, D., and Stemmler, K.: Measurements of OVOCs and NMHCs in a swiss highway tunnel for estimation of road transport emissions, Environ. Sci. Technol., 41, 7060–7066, 2007.

Lindinger, W., Hansel, A., and Jordan, A.: On-line monitoring of volatile organic compounds at pptv levels by means of proton-transfer-reaction mass spectrometry (PTR-MS) – medical applications, food control and environmental research, Int. J. Mass Spectrom., 173, 191–241, 1998.

Löndahl, J., Pagels, J., Boman, C., Swietlicki, E., Massling, A., Rissler, J., Blomberg, A., Bohgard, M., and Sandstrom, T.: Deposition of biomass combustion aerosol particles in the human respiratory tract, Inhal. Toxicol., 20, 923–933, 2008.

McMurry, P. H. and Rader, D. J.: Aerosol wall losses in electrically charged chambers, Aerosol Sci. Tech., 4, 249–268, 1985.

Miracolo, M. A., Hennigan, C. J., Ranjan, M., Nguyen, N. T., Gordon, T. D., Lipsky, E. M., Presto, A. A., Donahue, N. M., and Robinson, A. L.: Secondary aerosol formation from photochemical aging of aircraft exhaust in a smog chamber, Atmos. Chem. Phys., 11, 4135–4147, doi:10.5194/acp-11-4135-2011, 2011.

Monks, P. S., Granier, C., Fuzzi, S., Stohl, A., Williams, M. L., Akimoto, H., Amann, M., Baklanov, A., Baltensperger, U., Bey, I., Blake, N., Blake, R. S., Carslaw, K., Cooper, O. R., Dentener, F., Fowler, D., Fragkou, E., Frost, G. J., Generoso, S., Ginoux, P., Grewe, V., Guenther, A., Hansson, H. C., Henne, S., Hjorth, J., Hofzumahaus, A., Huntrieser, H., Isaksen, I. S. A., Jenkin, M. E., Kaiser, J., Kanakidou, M., Klimont, Z., Kulmala, M., Laj, P., Lawrence, M. G., Lee, J. D., Liousse, C., Maione, M., McFiggans, G., Metzger, A., Mieville, A., Moussiopoulos, N., Orlando, J. J., O'Dowd, C. D., Palmer, P. I., Parrish, D. D., Petzold, A., Platt, U., Poschl, U., Prevot, A. S. H., Reeves, C. E., Reimann, S., Rudich, Y., Sellegri, K., Steinbrecher, R., Simpson, D., ten Brink, H., Theloke, J., van der Werf, G. R., Vautard, R., Vestreng, V., Vlachokostas, C., and von Glasow, R.: Atmospheric composition change – global and regional air quality, Atmos. Environ., 43, 5268–5350, 2009.

Ng, N. L., Kroll, J. H., Chan, A. W. H., Chhabra, P. S., Flagan, R. C., and Seinfeld, J. H.: Secondary organic aerosol formation from *m*-xylene, toluene, and benzene, Atmos. Chem. Phys., 7, 3909–3922, doi:10.5194/acp-7-3909-2007, 2007.

Ng, N. L., Canagaratna, M. R., Zhang, Q., Jimenez, J. L., Tian, J., Ulbrich, I. M., Kroll, J. H., Docherty, K. S., Chhabra, P. S., Bahreini, R., Murphy, S. M., Seinfeld, J. H., Hildebrandt, L., Donahue, N. M., DeCarlo, P. F., Lanz, V. A., Prévôt, A. S. H., Dinar, E., Rudich, Y., and Worsnop, D. R.: Organic aerosol components observed in Northern Hemispheric datasets from Aerosol Mass Spectrometry, Atmos. Chem. Phys., 10, 4625–4641, doi:10.5194/acp-10-4625-2010, 2010.

Odum, J. R., Jungkamp, T. P. W., Griffin, R. J., Forstner, H. J. L., Flagan, R. C., and Seinfeld, J. H.: Aromatics, reformulated gasoline, and atmospheric organic aerosol formation, Environ. Sci. Technol., 31, 1890–1897, 1997.

Onasch, T. B., Trimborn, A., Fortner, E. C., Jayne, J. T., Kok, G. L., Williams, L. R., Davidovits, P., and Worsnop, D. R.: Soot particle aerosol mass spectrometer: development, validation, and initial application, Aerosol. Sci. Tech., 46, 804–817, 2012.

Pagels, J., Khalizov, A. F., McMurry, P. H., and Zhang, R. Y.: Processing of soot by controlled sulphuric acid and water condensation mass and mobility relationship, Aerosol. Sci. Tech., 43, 629–640, 2009a.

Pagels, J., Wierbicka, A., Nilsson, E., Isaxon, C., Dahl, A., Gudmundsson, A., Swietlicki, E., and Bohgard, M.: Chemical composition and mass emission factors of candle smoke particles, J. Aerosol. Sci., 40, 193–208, 2009b.

Paulsen, D., Dommen, J., Kalberer, M., Prevot, A. S. H., Richter, R., Sax, M., Steinbacher, M., Weingartner, E., and Baltensperger, U.: Secondary organic aerosol formation by irradiation of 1,3,5-trimethylbenzene-NO_x-H_2O in a new reaction chamber for atmospheric chemistry and physics, Environ. Sci. Technol., 39, 2668–2678, 2005.

Platt, S. M., El Haddad, I., Zardini, A. A., Clairotte, M., Astorga, C., Wolf, R., Slowik, J. G., Temime-Roussel, B., Marchand, N., Ježek, I., Drinovec, L., Močnik, G., Möhler, O., Richter, R., Barmet, P., Bianchi, F., Baltensperger, U., and Prévôt, A. S. H.: Secondary organic aerosol formation from gasoline vehicle emissions in a new mobile environmental reaction chamber, Atmos. Chem. Phys. Discuss., 12, 28343–28383, doi:10.5194/acpd-12-28343-2012, 2012.

Presto, A. A., Hartz, K. E. H., and Donahue, N. M.: Secondary organic aerosol production from terpene ozonolysis. 1. effect of UV radiation, Environ. Sci. Technol., 39, 7036–7045, 2005.

Robinson, A. L., Donahue, N. M., Shrivastava, M. K., Weitkamp, E. A., Sage, A. M., Grieshop, A. P., Lane, T. E., Pierce, J. R., and Pandis, S. N.: Rethinking organic aerosols: semivolatile emissions and photochemical aging, Science, 315, 1259–1262, 2007.

Samy, S. and Zielinska, B.: Secondary organic aerosol production from modern diesel engine emissions, Atmos. Chem. Phys., 10, 609–625, doi:10.5194/acp-10-609-2010, 2010.

Sato, K., Takami, A., Isozaki, T., Hikida, T., Shimono, A., and Imamura, T.: Mass spectrometric study of secondary organic aerosol formed from the photo-oxidation of aromatic hydrocarbons, Atmos. Environ., 44, 1080–1087, 2010.

Schauer, J. J., Kleeman, M. J., Cass, G. R., and Simoneit, B. R. T.: Measurement of emissions from air pollution sources, 5. C-1-C-32 organic compounds from gasoline-powered motor vehicles, Environ. Sci. Technol., 36, 1169–1180, 2002.

Schifter, I., Diaz, L., and Rodriguez, R.: Cold-start and chemical characterization of emissions from mobile sources in Mexico, Environ. Technol., 31, 1241–1253, 2010.

Song, C., Na, K. S., and Cocker, D. R.: Impact of the hydrocarbon to NO_x ratio on secondary organic aerosol formation, Environ. Sci. Technol., 39, 3143–3149, 2005.

Song, C., Na, K., Warren, B., Malloy, Q., and Cocker, D. R.: Impact of propene on secondary organic aerosol formation from *m*-xylene, Environ. Sci. Technol., 41, 6990–6995, 2007.

Taipale, R., Ruuskanen, T. M., Rinne, J., Kajos, M. K., Hakola, H., Pohja, T., and Kulmala, M.: Technical Note: Quantitative long-term measurements of VOC concentrations by PTR-MS – measurement, calibration, and volume mixing ratio calculation methods, Atmos. Chem. Phys., 8, 6681–6698, doi:10.5194/acp-8-6681-2008, 2008.

Weilenmann, M., Favez, J. Y., and Alvarez, R.: Cold-start emissions of modern passenger cars at different low ambient temperatures and their evolution over vehicle legislation categories, Atmos. Environ., 43, 2419–2429, 2009.

Weitkamp, E. A., Sage, A. M., Pierce, J. R., Donahue, N. M., and Robinson, A. L.: Organic aerosol formation from photochemical oxidation of diesel exhaust in a smog chamber, Environ. Sci. Technol., 41, 6969–6975, 2007.

Zhang, R. Y., Khalizov, A. F., Pagels, J., Zhang, D., Xue, H. X., and McMurry, P. H.: Variability in morphology, hygroscopicity, and optical properties of soot aerosols during atmospheric processing, P. Natl. Acad. Sci. USA, 105, 10291–10296, 2008.

Table 1. Initial experimental conditions.

Exp -ID	Type	Source	Initial C_6–C_9 light aromatics (ppb)	Initial NO (ppb)	Initial $(NH_4)_2SO_4$ ($\mu g\,m^{-3}$)	Total hydrocarbons (ppm)[*]
I1	Cold idling	Euro II	303	33	10	2.4
I2	Cold idling	Euro II	317	47	18	2.5
I3	Cold idling	Euro II	197	107	13	2.2
I4	Cold idling	Euro III	123	20[**]	15	1.0
I5	Cold idling	Euro IV	289	35	22	2.2
S1	Cold start	Euro IV	402	47	6	∼ 1
P1	Precursor	tol., m-xyl., 1,2,4-tmb	288	43	18	–
P2	Precursor	m-xyl.	250	38	19	–

[*] Measured with the FID.

[**] The given NO value is after addition of O_3 to convert NO to NO_2, the initial NO concentration prior to addition of O_3 was 125 ppb.

ACPD
12, 31725–31765, 2012

Table 2. Summary of the results and experimental conditions.

Exp. -ID	Initial LA to NO$_x$ ratio (ppbC/ppbN)	Formed ozone (ppb)	Reacted LA (C_6–C_9) ($\mu g\,m^{-3}$)	Emitted POA ($\mu g\,m^{-3}$)	Formed SOA ($\mu g\,m^{-3}$)	Apparent Mass Yield Y	Formed NO_3 ($\mu g\,m^{-3}$)
I1	55	111	138	2.9	21	0.15	9
I2	45	118	198	0.2	44	0.22	24
I3	13	156	264	0.1	51	0.19	71
I4	7	72	97	0.1	9	0.09	91
I5	53	102	62	0.2	5	0.09	4
S1	64	98	205	0.6	12	0.06	< 1
P1	49	86	462	–	53	0.12	2
P2	49	72	435	–	59	0.14	2

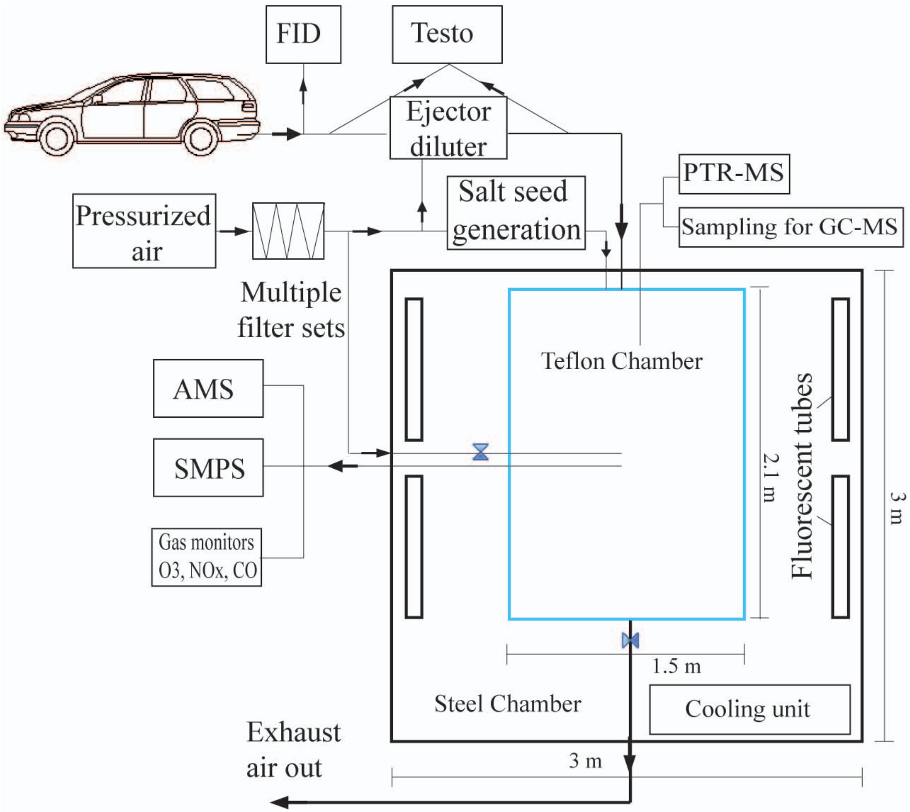

Fig. 1. Schematic representation of the smog chamber and dilution system, seen from above.

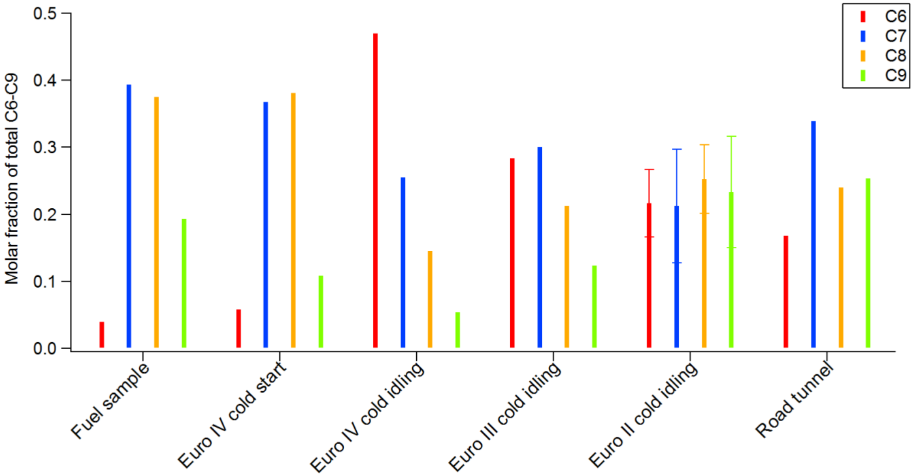

Fig. 2. The molar fraction of C_6–C_9 light aromatics (GC-MS) in the exhaust, a sample of the gasoline fuel used in the measurement campaign and VOC measurements in a road tunnel (Legreid et al., 2007). The whiskers indicate ±1 standard deviation (σ) of repeated measurements. Legreid et al. (2007) only measured 1,2,4-TMB, the total C_9 concentration is estimated from that number and the fraction of 1,2,4-TMB of total C_9 in our exhaust measurements.

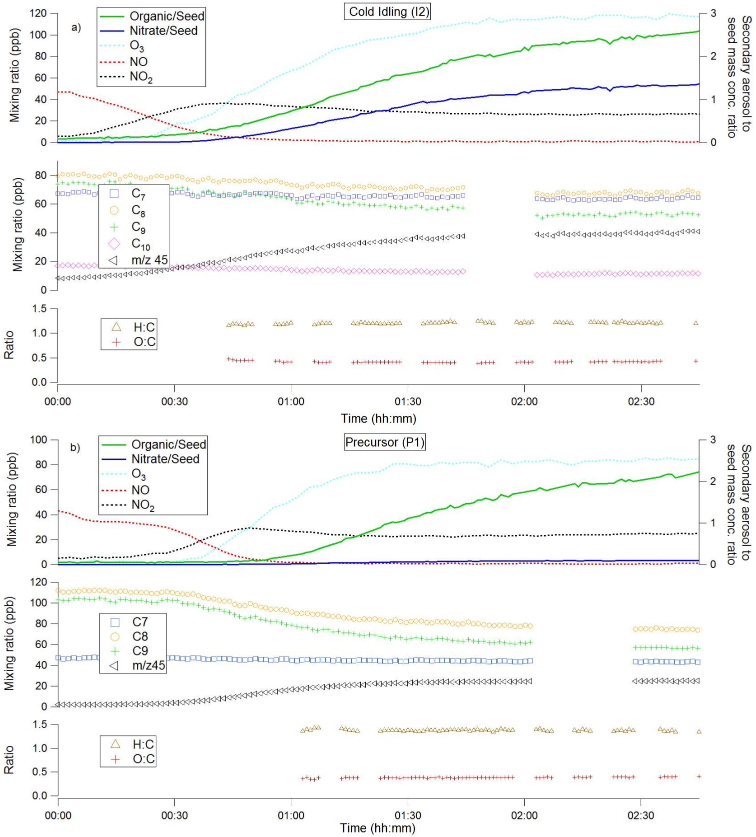

Fig. 3. Time resolved data from experiment I2 **(a)** and P1 **(b)**. The upper panels show the mixing ratios of NO, NO_2 and O_3 (left y-axis) and the mass concentration ratio between SOA, nitrate and seed aerosol on the right y-axis. The middle panels represent the mixing ratio of light aromatics (m/z 93: toluene, m/z 107: xylenes, m/z 121: C_9-aromatics, m/z 135: C_{10}-aromatics) and acetaldehyde (m/z 45). The lower graphs feature the H : C and O : C ratios extracted from elemental analysis of organic aerosol in high-resolution AMS data. The UV lights were turned on at Time = 00:00. Missing data points are either due to internal calibration (PTR-MS), thermodenuder measurements (AMS) or omitted on account of low mass loadings.

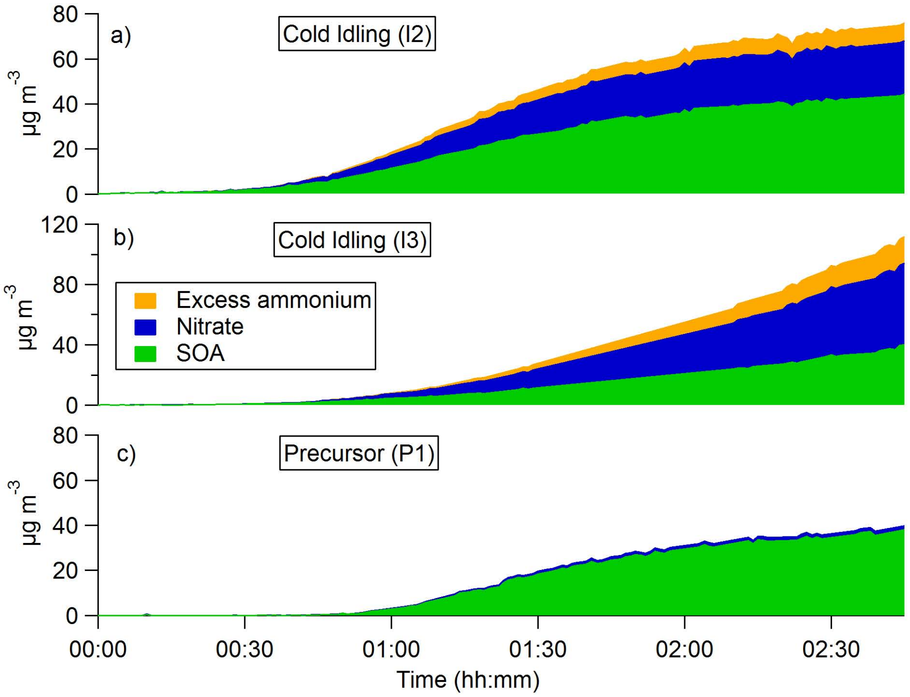

Fig. 4. Chemically resolved wall loss corrected mass concentration ($\mu g\,m^{-3}$) from AMS data from experiment I2 **(a)**, I3 **(b)** and P1 **(c)**. The ammonium sulfate seed has been subtracted. The reported ammonia is excess ammonia not bound to sulfate, thus indicative of ammonium nitrate formation. Time = 00:00 indicates the start of the UV radiation.

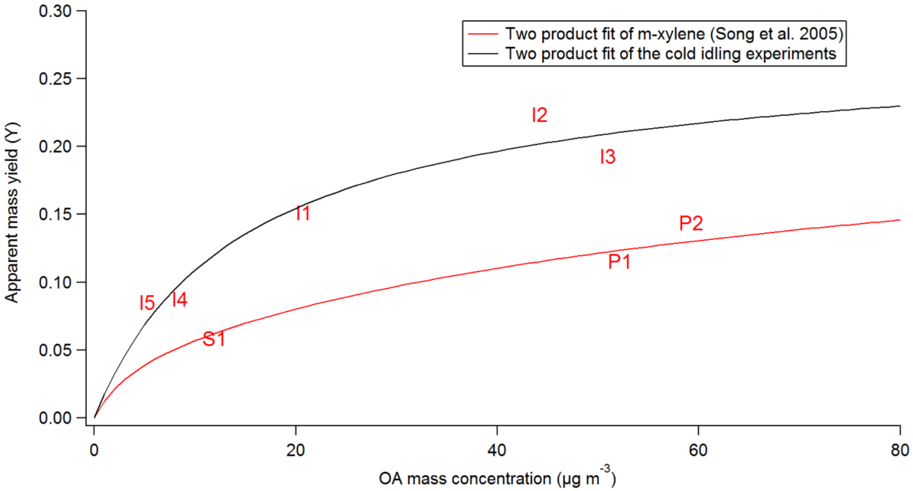

Fig. 5. The apparent mass yield (Eq. 2) from the gasoline experiments plotted against the concentration of organic aerosol mass. The black line represents a two product fit, $(Y = C_{\mathrm{OA}} \cdot \left[\left(a_1 \cdot k_1 / (1 + k_1 \cdot C_{\mathrm{OA}})\right) + \left(a_2 \cdot k_2 / (1 + k_2 \cdot C_{\mathrm{OA}})\right)\right]$, where $a_1 = 0.254$, $a_2 = 0.048$, $k_1 = 0.072$ and $k_2 = 0.005$) to the apparent mass yield for experiment I1–I5. The red line is a two product fit to the *m*-xylene yield from Song et al. (2005), (scaled by 0.88 and assuming a density of 1.4 $\mathrm{g\,cm^{-3}}$) to fit the precursor experiments carried out in this study. I1–I5 represents cold idling, S1 cold start and P1–P2 the precursor experiments.

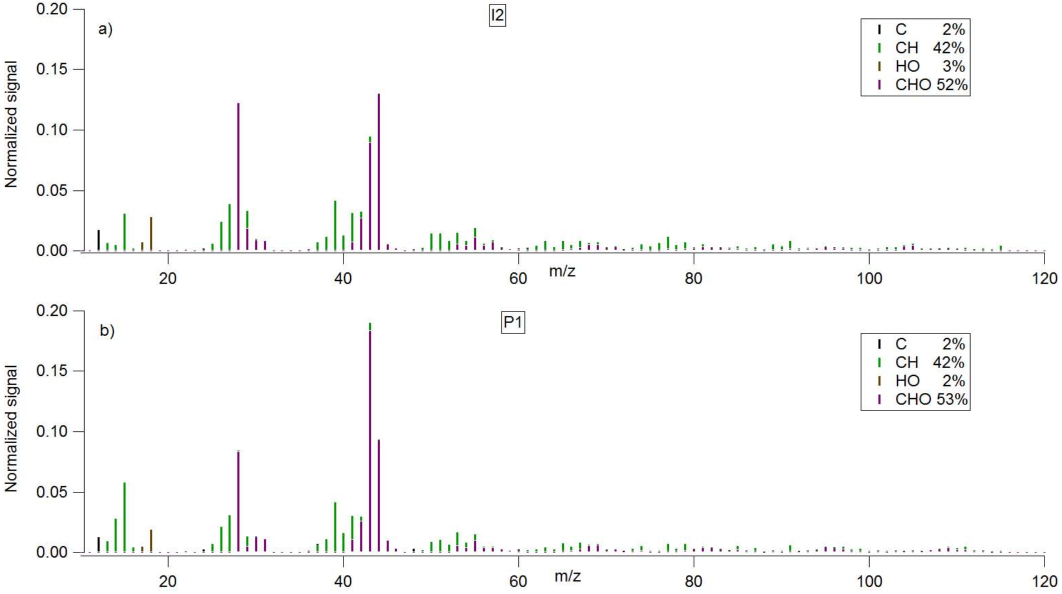

Fig. 6. Normalized high resolution MS of OA at the end of gasoline exhaust experiment I2 **(a)** and precursor mixture experiment P1 **(b)** (toluene, *m*-xylene, 1,2,4 TMB). The ion fragments detected have been grouped into four families; C containing only carbon; CH containing only carbon and hydrogen; HO containing only oxygen and hydrogen; and CHO containing carbon, hydrogen and oxygen (with the exception of CO_2^+ which dominates at m/z 44). The POA contribution in experiment I2 was < 0.5 %.

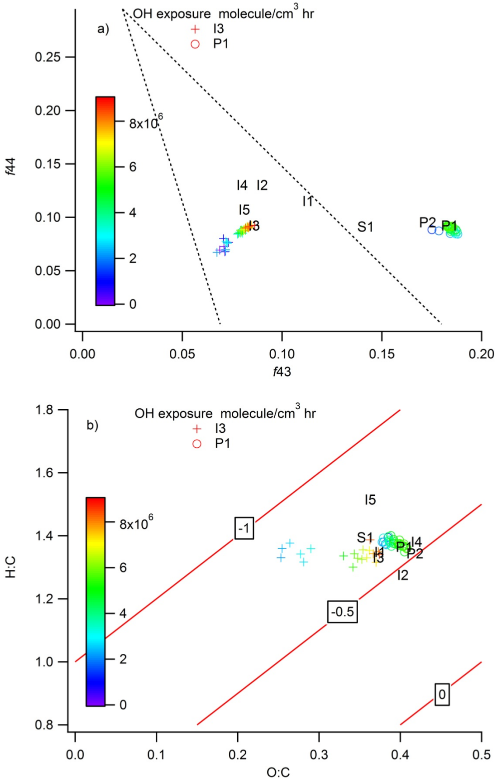

Fig. 7. (a) The mass fraction of organic signal at m/z 44 ($f44$) vs m/z 43 ($f43$) at the end of each experiment, **(b)** H : C vs O : C of the OA at the end of each experiment. The triangular space in **(a)** indicates the range which covers the majority of atmospheric OOA observations (Ng et al., 2010). The diagonal lines in **(b)** indicate estimated average carbon oxidation states −1, −0.5 and 0 (Kroll et al., 2011). For experiments I3 (+) and P1 (o) time resolved data are shown colored by OH exposure. The cumulative OH exposure was 8.5×10^6 molecule cm^{-3} h in I3 and 6.4×10^6 molecule cm^{-3} h in P1.

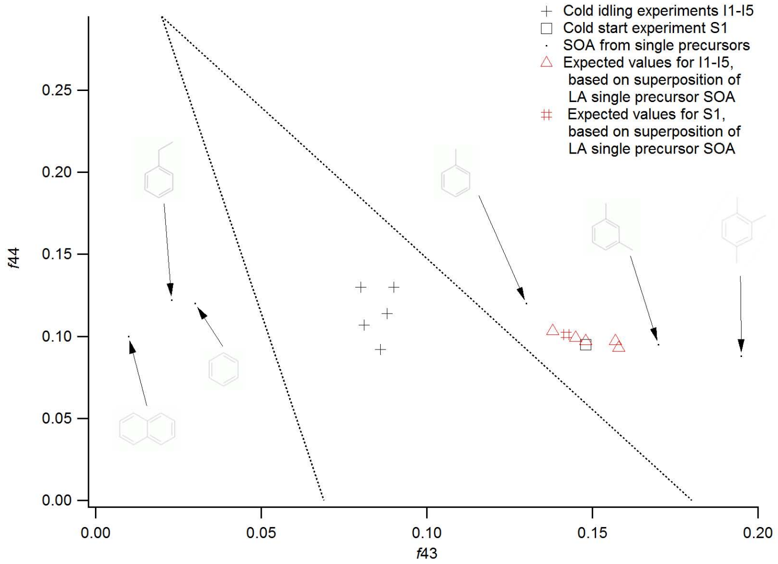

Fig. 8. The $f43$, $f44$ for experiments I1–I5 (+) and for SOA formed from single precursors; LA and naphthalene plotted together with the triangle from Ng et al. (2010). Also plotted are expected values for I1–I5 if only LA contribute to SOA formation, assuming superposition of single precursor SOA. For experiment I1 and S1 which had non negligible POA contribution to OA, the SOA values have been calculated from the total OA assuming non-volatile POA with a constant composition through the whole experiment. The $f44$ to $f43$ of SOA from precursors featured in the figure are retrieved from the following sources: benzene (Ng et al., 2010), toluene (Chhabra et al., 2011), ethylbenzene (Sato et al., 2010) *m*-xylene (experiment P2, this study), 1,2,4-trimethylbenzene (derived from exp. P1) naphthalene (Chhabra et al., 2011). The results suggest no more than 60 % of SOA in I1–I5 were due to C_6–C_9 LA precursors, assuming that the MS of gasoline exhaust SOA can be estimated as a weighted mean of the MS of SOA from single precursors. See Table S4 (Supplement) for more details about these calculations.